Imaging complex model catalysts in action: From surface science towards industrial practice using high-pressure scanning tunneling microscopy

Mom, R.V.

Chapter 5

Simultaneous scanning tunneling microscopy and synchrotron X-ray measurements in a gas environment

A combined X-ray and scanning tunneling microscopy (STM) instrument is presented that enables the local detection of X-ray absorption on surfaces in a gas environment. To suppress the collection of ion currents generated in the gas phase, coaxially shielded STM tips were used. The conductive outer shield of the coaxial tips can be biased to deflect ions away from the tip core. In tunneling contact, the X-ray-induced current is separated from the regular topographic tunneling current using a novel high-speed separation scheme. We demonstrate the capabilities of the instrument by measuring the local X-ray-induced current on Au(111) in 800 mbar Ar.

5.1 Introduction

The synchrotron-based techniques developed over the last decades provide a powerful toolbox for the study of interface phenomena. The weak interaction of X-rays with matter makes these methods particularly suitable for *operando* studies, which are indispensable in research areas such as catalysis [1], environmental science [2], and film growth [3]. However, most X-ray techniques make use of a large beam spot compared to the features studied, thereby averaging out possibly important structural and chemical variations. For techniques that use a highly focused beam on the other hand, finding the feature of interest can be a tedious process as searching based on reciprocal-space images or absorption features is non-trivial.

Scanning probe microscopy can supplement X-ray measurements by providing local structural information in real space. Inspired by this potential, several atomic force microscopes (AFM) [4–9] and scanning tunneling microscopes (STM) [10–14] have been installed on beamline end stations. In the AFM studies, it was shown that the AFM tip can be used to align the X-ray beam with features of interest [6]. Once aligned, the tip can be used for nano-manipulation or the application of local stress [15,16].

Using the combination of STM and X-rays, it was shown that the current collected by the STM tip can be used to measure local X-ray absorption, with a spatial resolution as small as 2 nm [11,17–19]. Thus, local chemical information can be obtained and coupled to the local structure. This combination is highly desirable for the understanding and design of materials and chemical processes.

So far, all synchrotron X-ray assisted STM (SXSTM) studies have been performed in vacuum. Under these conditions, the signal collected by the tip consists of three principal components: the photo-electron current, the regular topographic tunneling current, and an X-ray-induced increase of the tunneling current. While both the photo-electron current and the X-ray-induced increase of the tunneling current are related to X-ray absorption, only the latter provides local information [11,17–19]. To improve the ratio between this local signal and the photo-electron current, most SXSTM experiments employ insulator-coated STM tips, leaving only the tip apex uncoated [17,20–23]. This effectively reduces the number of photo-electrons that the tip collects. Besides this background reduction, the X-ray-induced part of the tunneling current needs to be separated from the regular tunneling current. Several experimental schemes employing a beam chopper and lock-in amplification have been developed for this purpose [11,24].

To use SXSTM in *operando* studies at elevated pressures, two challenges need to be addressed: i) Inhibitively large ion currents are generated in the gas phase. We show that insulator-coated tips are inadequate to suppress these. ii) Most interesting systems for *operando* studies require elevated temperatures and have some degree of roughness in their morphology. To cope with thermal drift and to follow the surface morphology accurately, fast response in the height feedback is necessary. However,

the current separation schemes for the regular and the X-ray-induced tunneling current limit the height feedback in the STM to response frequencies below roughly 1 kHz.

Here, we describe an instrument that can perform SXSTM measurements in a gas environment using hard X-rays, overcoming the barriers for performing *operando* studies. Our methodology provides several novelties: i) A quick method for aligning tip and beam with micrometer precision. ii) An electronics scheme to separate X-ray-induced current and regular tunneling current that enables fast height feedback at frequencies up to the chopper frequency. iii) A coaxially shielded STM tip and mounting configuration that effectively suppresses the ion current background. As a proof of concept, we have collected the local, X-ray-induced tunneling current on a Au(111) sample at a gas pressure of 800 mbar.

5.2 Instrument design

5.2.1 High-pressure cell

The starting point for our experiments was the high-pressure scanning probe and surface X-ray scattering instrument developed earlier in collaboration between our group and the ID03 beamline staff at the ESRF [14], which we modified for the SXSTM measurements. In short, this system consists of an ultrahigh vacuum (UHV) chamber with a high-pressure cell on top (see Figure 5.1) [25]. The UHV chamber allows for surface preparation by ion bombardment, annealing, controlled gas exposure, and metal evaporation onto the sample. The high-pressure cell can be operated as a flow reactor, providing a controlled gas atmosphere at pressures up to 1.1 bar. The cell is exchangeable, allowing for a versatile combination of experiments.

In our recent work, we fitted a high-pressure scanning probe module on the system [14,26]. Similar to the design of the ReactorSTM and ReactorAFM [27,28], it uses a single piezo tube both for the coarse approach of the tip to the sample and for generating the scanning motion. The coarse approach is achieved by a stick-slip motion of the tip holder (slider) on two tracks. The piezo tube is separated from the gas environment by a polyimide cap and a viton seal, as depicted in Figure 5.1b. In our previous design, the reactor wall was a dome-shaped aluminum piece of 1 mm thickness, providing homogeneous and satisfactory X-ray transmission over a large range of angles at photon energies above 18 keV. While this made the system excellent for surface X-ray diffraction measurements, the X-ray transmission was insufficient in the lower energy range relevant to X-ray absorption spectroscopy.

To allow for measurements at energies down to 8 keV, we designed a new cell that uses four thin, exchangeable windows (see Figure 5.1) sealed on both sides by viton O-rings. In our first test measurements, we used a stack of three 75 µm thick Kapton sheets for each window. In the energy range from 10 keV to 12 keV, the Kapton stack provides an excellent X-ray transparency of 91% to 95% [29]. However, the

permeability of Kapton towards gases [30] limits the base pressure of the UHV chamber to the 10^{-6} mbar range. Aluminum foil windows provide a lower transmission (59% for 100 µm thick foil at 11 keV [29]), yet do not suffer from any gas permeability. Beryllium windows were not preferred here for safety reasons, as the reactor needs to be handled frequently for tip exchanges.

The reactor walls and the part of the microscope head that are exposed to gases are gold coated. This prevents undesirable side reactions from occurring on these surfaces. Furthermore, charge collected on the walls from photo-electrons and ions is immediately neutralized. Charging of the native oxide of materials such as aluminum and stainless steel may cause memory effects in the background signal of the SXSTM measurements. This could adversely affect the reproducibility of the data.

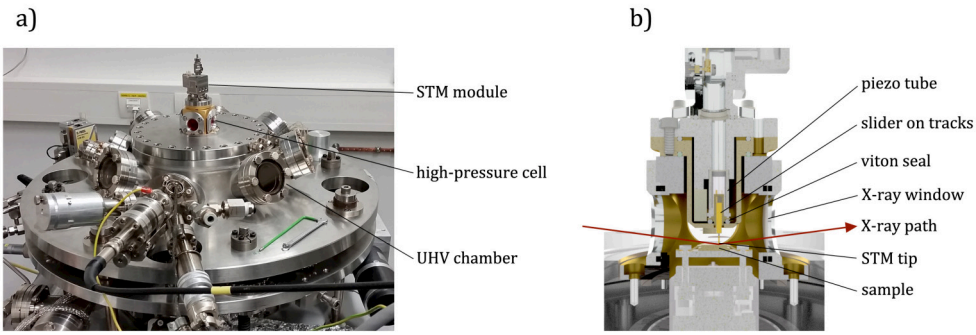

Figure 5.1: Overview of the set-up. a) Assembly of ID03's ReactorSXRD chamber [25], our new high-pressure cell and the recently developed STM module [14]. b) Cross-section of the STM module and high-pressure cell.

5.2.2 Coaxial tips and mounting scheme

In a gas environment, the X-ray-induced current collected by the STM tip behaves differently as compared to the vacuum situation. Photo-electrons emerging from the sample cause a cascade of ionization processes in the gas. This effect is particularly pronounced for the high-energy Auger electrons produced during hard X-ray absorption [31,32]. Furthermore, the plasma created in the gas environment helps the charge transport to and from insulating surfaces [33–35]. Hence, when a beam chopper is employed, this may generate oscillating electric fields that can couple into the tunneling current. These effects cause a complex behavior of the background signal in SXSTM measurements, making reproducibility of experiments difficult. It is therefore essential to minimize the background current.

To achieve this reduction in background, we fabricated both insulator-coated and coaxially shielded STM tips. The latter consist of a conductive core, an insulating layer, and a conductive outer layer (shield), as shown in Figure 5.2. While the core is

used for measuring the tunneling current, the shield layer neutralizes ions. Tips are mounted such that the shield potential can be controlled independently with respect to the tip core and the sample, thus creating an electric field that deflects ions away from the tip core.

The insulator-coated tips were fabricated by a combination of SiO_2 sputter deposition and focused ion beam milling similar to that reported in literature [20,22,23]. The fabrication of coaxially shielded tips is less well established [17], hence we explored several preparation methods. As core material, we have used an electrochemically etched $Pt_{0.8}Ir_{0.2}$ wire (ø 0.25mm, Goodfellow). Three different types of insulation layer were tested: i) 100 nm SiO_2 prepared by atomic layer deposition (ALD) through 1100 cycles of bis(diethylamido)silane (Sigma-Aldrich SIBDEA) exposure and an O_2 plasma as co-reactant at 200 °C. ii) 1000 nm SiO_2 prepared by plasma-enhanced chemical vapor deposition (PE-CVD) using a plasma of silane and O_2 at 300 °C. iii) Polymer coating prepared by pushing the tip through a droplet of polyethylene-vinylacetate-based glue gun wax at 80 °C, a method commonly used for electrochemical STM [36].

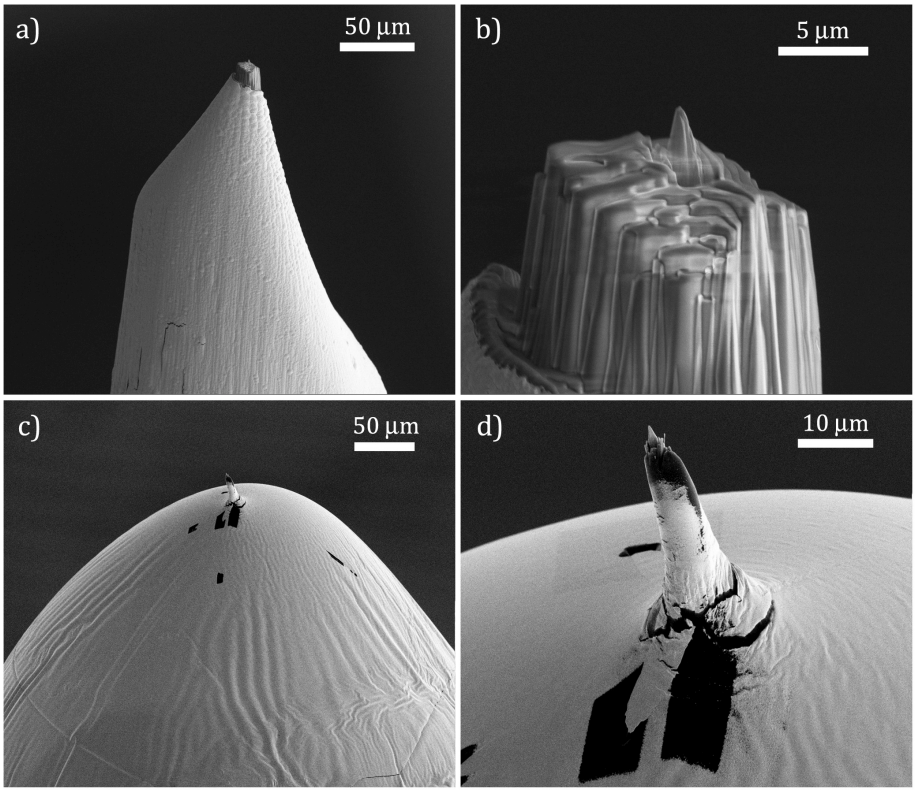

Figure 5.2: Scanning electron microscopy (SEM) images of coaxially shielded STM tips. a,b) $Pt_{0.8}Ir_{0.2}$ with SiO_2/Au coating. c,d) $Pt_{0.8}Ir_{0.2}$ with polymer/Au coating.

In all three cases, >2 MΩ core-shield insulation was accomplished with a success rate of over 50%. For the ALD tips, the coating was very homogeneous but too fragile to survive further assembly. For the PE-CVD tips, the insulation thickness was not uniform over the tip due to inhomogeneities in the plasma that are common around conducting three-dimensional objects inserted into the plasma. As a result, the coating at the apex was 7.5 µm thick while the average was only 1 µm. For the polymer-coated tips, the coating thickness decreased from 1 mm halfway the tip to a few hundred nanometer at the apex (see Figure 5.2).

The shield coating was applied by radiofrequency sputter deposition of a Ti seed layer followed by 500 nm Au for the ALD and PE-CVD tips and 100 nm Au for the polymer tips. Subsequently, the apex was shaped using focused ion beam milling. In this process, the original tip apex was first cut off, followed by a donut-shaped ion milling pattern around the new tip apex to remove the last ~1 µm of the isolation and shield layers, so that the core protrudes (see Figure 5.2). Using a finer donut shape, the apex was sharpened.

The mounting configuration of the coaxial tips is depicted in Figure 5.3. Essential in the design is that the core and shield of the tip have separate electrical connections. Furthermore, the pick up of ion current by the tip holder needs to be minimized. To achieve this, a gold-coated Kapton foil was attached to the tip using non-conductive glue. Subsequently, the Au coating of the Kapton foil was connected to the shield of the coaxial tip using Agar silver paint. Similarly, a thin Au-coated tungsten wire was contacted to the Au coating of the Kapton through a puncture in the foil. This wire and the tip core were mounted on the tip holder (slider), which consists of two electrically isolated pieces of Au-coated machine steel. Each piece makes contact to one of the tracks on the piezo motor. Shielded wires provide connections from to the two tracks to outside of the reactor.

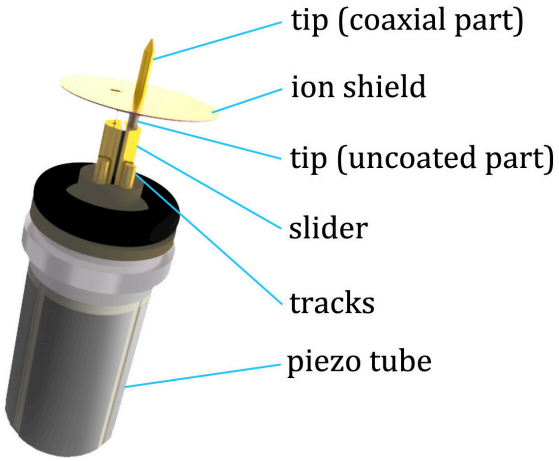

Figure 5.3: Mounting configuration of the coaxial tip.

After tip fabrication and mounting, a typical resistance of 2 GΩ between tip core and shield could be achieved, allowing for a shield bias of several volt with respect to the core. Thus a strong electrical field between the tip shield and the sample can be applied, deflecting both positive and negative charges before they can reach the tip core.

5.2.3 Tip-beam alignment

All experiments were conducted at the ID03 beam line at the European Synchrotron Radiation Facility (ESRF). The beam was focused to 25 μm × 25 μm using a toroidal mirror. In the energy window employed, 10 keV to 13 keV, a flux of 10^{13} photons/s was delivered to the sample in the reactor cell with Kapton windows. For the Al dome reactor developed in our previous work [14], the flux on the sample was around 10^{11} photons/s.

In order to align the STM tip with the X-ray beam, the chamber was placed on a hexapod, which in turn stands on a six-circle diffractometer. This allows translation in x (horizontal, perpendicular to the beam), y (parallel to the beam), and z (vertical), as well as tilting and rotation. We used the shadow of the STM tip on the Maxipix X-ray detector [37] as a probe for the alignment. First, the tip was brought to within a few micrometer from the sample surface. With the beam parallel to the sample surface, the chamber height (z) was set such that half of the beam was blocked by the sample. When the chamber is then translated in x, it passes through the configuration in which the beam hits the tip, casting a shadow on the detector. Figure 5.4a depicts the intensity of the beam spot on the detector recorded during such a chamber translation scan. The minimum of this curve is located at the position where the tip maximally blocks the beam, as is also evidenced by the tip shadow that can be seen in the X-ray detector images (see Figure 5.4c) and the reflections from the sides of the tip. In order to align in both lateral directions, the chamber was rotated by 90° and the same scan was performed.

To confirm the accuracy of this method, a similar scan was performed with the X-rays incident on the sample at 0.5°. In this case, the beam reflected from the sample is recorded, which can also be blocked by the tip. Simultaneously, the photo-electron current on the tip core was measured. As shown in Figure 5.4b, the mismatch between the current maximum and the maximal beam blocking by the tip is only a few micrometer. The origin of this slight mismatch is likely the asymmetry of the tip on the scale of the beam spot, which is also apparent in Figure 5.4c.

5.2.4 Electronics scheme for separating the regular from the X-ray induced tunneling current

To obtain the local X-ray absorption signal, the X-ray beam is chopped [11,24]. Without adjustments to the height-feedback mechanism, which uses the tip current as an input, this would result in an oscillation of the tip height. In principle, the height

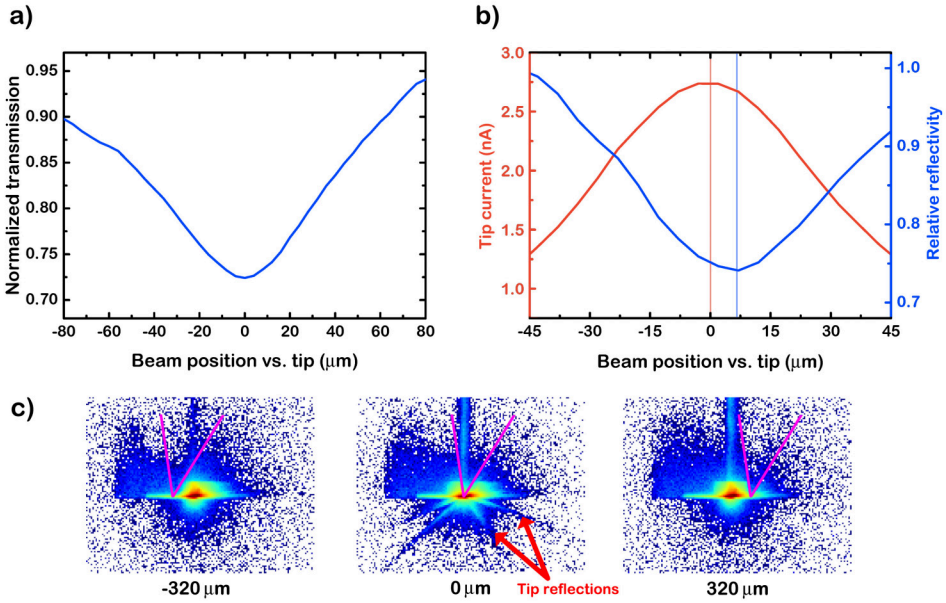

Figure 5.4: Alignment of STM tip and X-ray beam (tip-sample distance: ~ 3 μm). a) Transmission when moving the beam across the tip apex (beam parallel to sample). b) Tip current and X-ray reflection intensity when moving the beam across the sample underneath the tip (0.5° incidence). c) Beam spot on the detector when moving the beam across the tip. The purple lines indicate an estimate of the tip apex profile.

signal can be lock-in amplified to find the local X-ray absorption signal. However, the height signal has a logarithmic dependence on the tip current, making it relatively insensitive to the X-ray induced signal.

An alternative was proposed by Wang *et al.* [24], who performed height feedback on the tip current only after applying a low-pass filter. In this case the photo-induced signal is obtained from the tip current before the low-pass filter using lock-in amplification. In order to completely remove photo-induced effects from the height feedback, the photo-current signal from the lock-in amplifier is scaled and subtracted from the low-pass-filtered tunneling current. While this scheme allows for stable tunneling, the height feedback is limited to frequencies of maximally 0.1 × chopper frequency. The bandwidth of the high-gain preamplifiers used in STM restrict the chopper frequency to roughly 10 kHz, leading to a maximal feedback frequency of 1 kHz. This is adequate for flat surfaces and slow data acquisition in environments with low vibrational noise levels. However, more flexibility is desired for the nanoparticle systems typically used in catalysis. Furthermore, the challenging boundary conditions resulting from the integration of an STM in a reactor end-station impose limitations to the vibrational noise reduction that can be achieved [14].

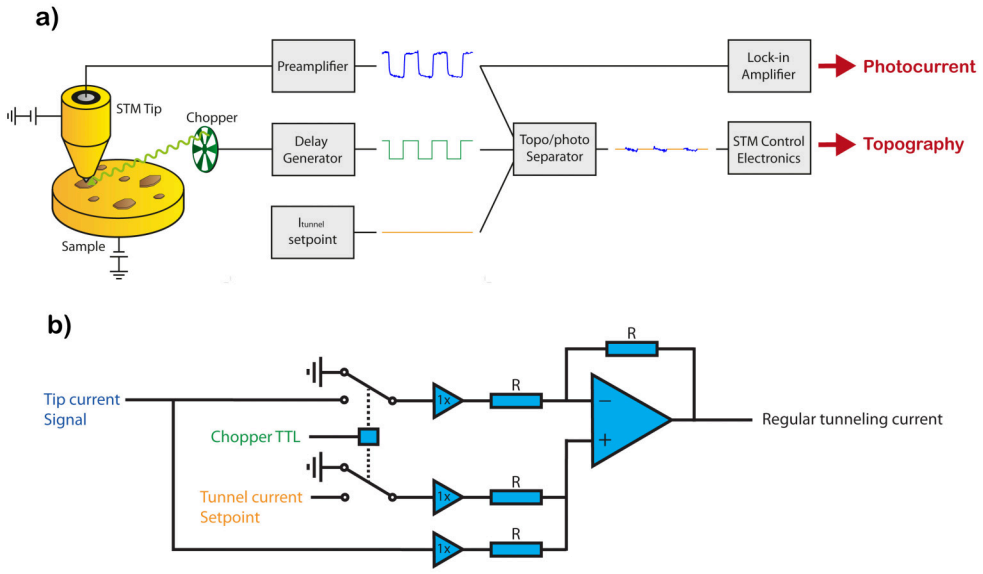

Figure 5.5: a) High-speed separation scheme for the regular tunneling current and the X-ray-induced current. b) Electronic circuit for the topo/photo separator, generating the input for the STM control system without X-ray-induced contributions.

In order to perform faster height feedback, we have developed a new scheme to separate the X-ray-induced current from the regular tunneling current. In essence, our circuit switches the height feedback off during the "beam on" phase of the X-ray chopper. This is accomplished by replacing the measured signal by the tunneling current setpoint during this phase. To do this, the transistor-transistor logic (TTL) signal from the beam chopper is fed into a delay generator, with which the phase and the duty cycle of the TTL signal can be adjusted independent of the phase and duty cycle of the chopper. Thus, the TTL phase can be matched to that observed in the tip signal. Adjusting the TTL duty cycle to prolong the "feedback off" period can be useful if the tip signal is not a perfect square wave, as is the case for our measurements in a gas environment.

The modified TTL signal is used in a purpose-built circuit (Figure 5.5b), which performs the following operation:

Output = Tip current + TTL × (Tunneling current setpoint - Tip current)

The output signal can be used for height feedback at frequencies up to the chopper frequency. In principle, the X-ray-induced signal could be obtained in a similar fashion. However, lock-in amplification of the tip signal provides a better signal-to-noise ratio.

We have first tested the acquisition scheme described above using the X-ray-induced current measured with the tip out of tunneling contact. From the data in 5. 6, it is clear that the X-ray-induced current is effectively removed from the regular signal. At high chopper frequencies, the signal deviates from the ideal square wave. Nevertheless, Figure 5.6b shows that the X-ray induced current can still be completely removed by changing the duty cycle of the TTL signal, thus evidencing the robustness of our scheme.

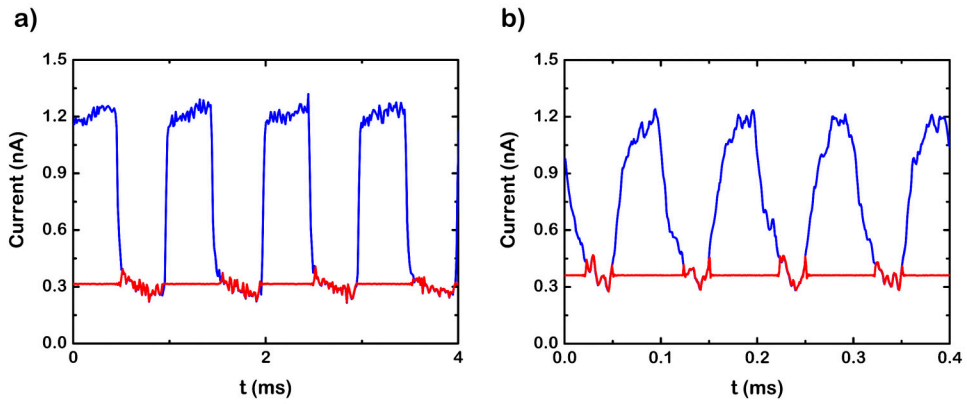

Figure 5.6: Test of the topo/photo current splitter using the X-ray-induced current with the tip out of tunneling contact in 1 bar O_2. The blue and the red curves show the signal before and after the separation circuit, respectively. a) Chopper at 1kHz b) Chopper at 10 kHz.

5.3 Performance

5.3.1 Current contributions from the gas environment

We have studied the SXSTM background currents generated by photo-electrons and ions by comparing the currents measured with a coaxial tip out of tunneling contact above a Au(111) surface in Ar, O_2 and in a modest vacuum of approximately 1 mbar. Although it is clear that many ionization events occur in the gas phase [31,32], it is not evident how these translate into the detection of a net current. We observed that the background current exhibits complex behavior, which is strongly dependent on many parameters. For instance, the current measured on the tip core at large tip-sample distances was clearly much higher in Ar than in O_2 (see Figure 5.7a). In contrast, at a tip- sample distance of only a few micrometers, the current was slightly higher in O_2. In general, the tip current was higher in a gas environment than in vacuum.

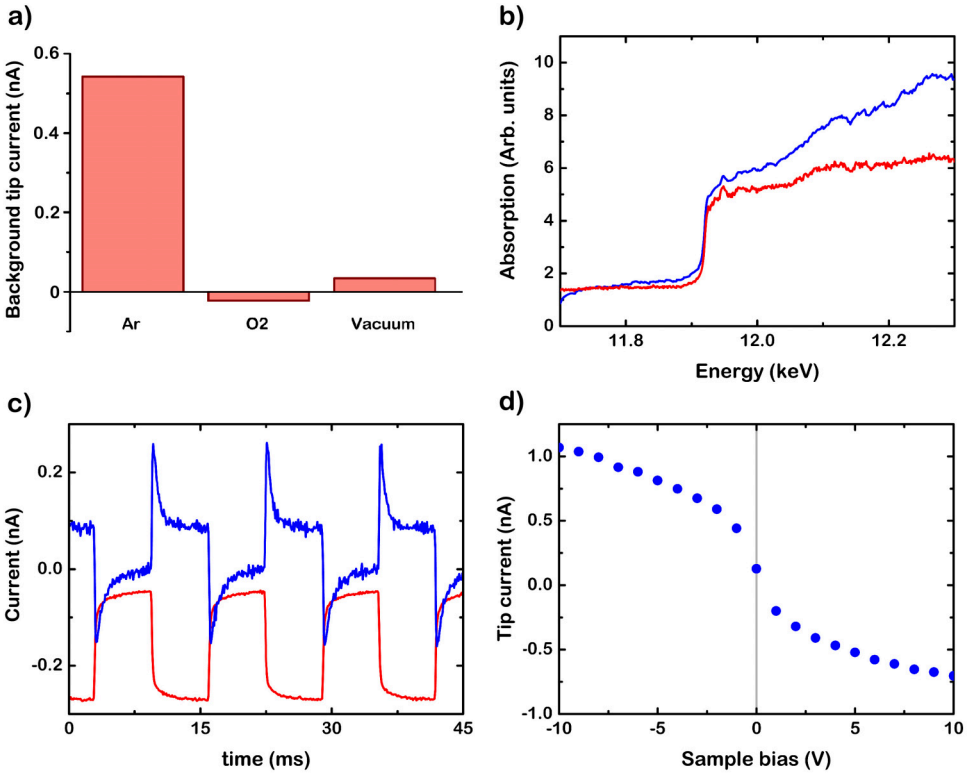

Figure 5.7: Characteristics of the SXSTM background currents in a gas environment, recorded with the tip out of tunneling contact. a) Background current on the tip in various environments at a photon energy of 12.3 keV for a tip-sample distance of 0.8 mm and a sample bias of -1 V. The Ar or O_2 pressure was 800 mbar, while 'vacuum' corresponds to a residual pressure of approximately 1 mbar. b) Au L3 edge absorption spectra from the fluorescence signal on the X-ray detector (red) and the tip current (blue), recorded in 800 mbar Ar. c) Sample current (red) and tip current (blue) in 500 mbar O_2 with the beam chopped at 80 Hz in an uncoated reactor, recorded with a SiO_2/Mo tip without Au shield. d) Dependence of the background signal on the sample bias, recorded in 800 mbar Ar.

From the Au L3 edge absorption spectrum in Figure 5.7b, it is clear that the tip current follows the absorption coefficient, apart from a difference in background slope. This is expected, as ion current collection is commonly used in conversion electron yield X-ray absorption spectroscopy [32]. Similarly, when changing the beam intensity (data not shown) the current-intensity relation only slightly deviates from linearity. In contrast, severe signal distortions can be observed in time-dependent measurements, when the beam is chopped. Figure 5.7c shows an example where the distortions occur both in the sample current and in the tip current. The origin of these distortions is likely related to charging and discharging of insulating surfaces in the reactor, which is accelerated in the presence of a gas environment [33–35]. For the measurement in Figure 5.7c, the Al dome reactor (with an insulating native oxide) was used, together

with a SiO_2-coated Mo tip without a conductive shield. Hence, charging/discharging may also occur on the insulating coating of the tip, strongly coupling into the tunneling current signal. This explains why the distortions are much more pronounced for the tip than for the sample. X-ray absorption by the gas was not a major contributor to the background currents, as was shown by measurements with the beam passing through the reactor without hitting the sample.

Figure 5.7d shows that the background current of the tip depends on the applied sample bias. For non-zero bias, the positively and negatively charged species generated by ionization events in the gas phase are separated by the electric fields between the sample, the tip and the reactor walls. The lack of precise symmetry in the tip current may be related to the fact that a net positive current is injected into the gas phase from the sample. As Figure 5.7a shows however, the current sign may also be inverted for different gases, again underlining the complexity of the charge dynamics in the background currents.

5.3.2 Background reduction using coaxial tips

To test the effectiveness of the coaxial STM tips described in Section 5.2.2, which consist of a conductive core and shield separated by an insulation layer, we simultaneously measured the current on the tip shield and on the core. As can be seen in Figure 5.8a, the maximum shield current is two orders of magnitude higher than that of the core. When the beam is placed more than 150 μm away from the tip, the core is completely insensitive towards the X-rays. In this situation, the electric field between tip shield and sample is sufficient to deflect all ions and electrons so that they cannot reach the tip core.

In many SXSTM studies, the STM tips were coated with an insulation layer only, not with a conductive outer shield [20–23]. While this can be adequate in UHV, Figure 5.7c shows that charging/discharging effects can cause signal distortions in a gas environment. The details of the shape of the distortions depend strongly on the precise beam-tip alignment and the gas environment, which makes it difficult to reproduce results. Hence, it is essential to use STM tips with a conductive outer shield for performing SXSTM measurements in a gas environment.

From Figure 5.6 it is clear that the coaxial tips provide the required improvement, since the square wave signal is only mildly distorted. It should be noted, however, that the magnitude of the background signal is still in the nA range and varies strongly from tip to tip. The type of insulation layer is not the most important factor, as the polymer-coated tips produced both the best and the worst background. Most likely, the geometrical variation at the tip apex is a major contributor to the observed differences between tips.

In addition to the fast signal distortions of the square wave, some Au/polymer-coated tips showed a slowly increasing offset current, which builds up during several minutes

after switching on the beam and can reach values of several hundred pA. The origin of this offset current must be a slow charging effect, which we have not been able to identify further. However, once the offset current has stabilized, it does not interfere with the SXSTM measurements.

To further reduce the background current, we applied a bias voltage to the shield. Figure 5.8b shows the effect of the bias on the X-ray-induced current received by the tip core. The current was corrected for the leakage current baseline in the absence of X-rays (2 GΩ shield-core resistance). Clearly, a small positive bias of ~0.5 V on the shield strongly reduces the background current. Surprisingly, at negative or larger positive shield bias, the background is not effectively reduced or even amplified. This could be due to surface conduction induced by ions landing on the exposed part of the tip insulation layer, as this would increase the leakage current between shield and core.

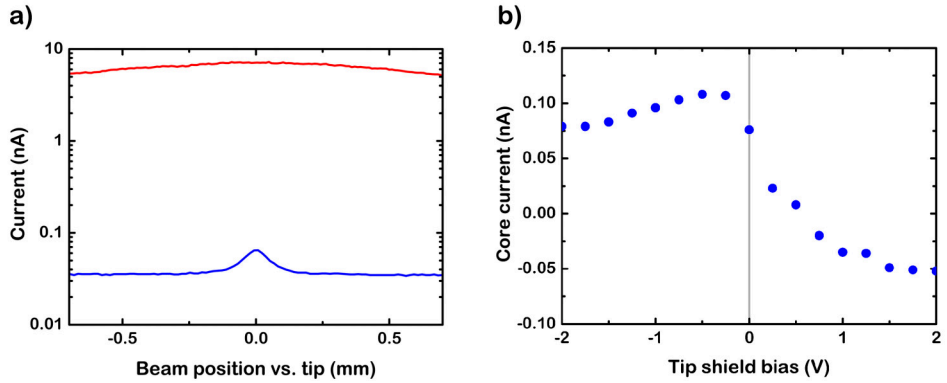

Figure 5.8: Effectiveness of the background reduction. a) Tip core (blue) and shield current (red) when scanning the beam across the tip in 1 bar O_2 at a tip-sample distance of 10 µm. Sample bias: -1 V, tip shield bias: 0 V b) Tip core current versus tip shield bias in 800 mbar Ar.

5.3.3 Imaging

A requirement in SXSTM measurements is that the tip is sufficiently sharp to properly image the surface: the height resolution should suffice to see atomic height steps and the lateral resolution should be better than 2 nm in order to identify nanoparticles. Figure 5.9 shows that atomic step resolution on Au(111) was indeed obtained with a Au/polymer coaxial tip in a beam chopped at 10 kHz. Line scans at higher magnification show that the Au(111) steps are imaged with a width of roughly 1 nm. Hence, the tip is sufficiently sharp to meet the lateral resolution criterion.

However, interference is clearly visible in Figure 5.9, decreasing the practical lateral resolution to approximately 5 nm. Nevertheless, spectral analysis of the tip current signal showed that the 10 kHz chopping frequency was effectively removed by the

topo/photo separator described in Section 5.2.4. Rather, the interference is caused by vibrational and electronic sources coupling into the signal, which are also present in regular STM mode without X-rays and the topo/photo separator. Because the STM was originally designed for X-ray scattering experiments, which require precise control over the incident angle and sample height, the STM could not easily be equipped with a vibrational isolation stage [14]. Improvements to suppress the interference are currently under development.

To get a lower bound estimate of the feedback responsivity, we scanned across a Au step edge with a tip repositioning speed of 5000 nm/s. Because the lateral width of the step edge feature is ~1 nm with the Au/polymer tip, the height feedback system needs to respond with a frequency of minimally 5 kHz in order to prevent a collision with the step edge. Since no tip-sample collisions occurred, it is clear that the topo/photo current separator allows for height feedback frequencies that are unfeasible with other separation schemes.

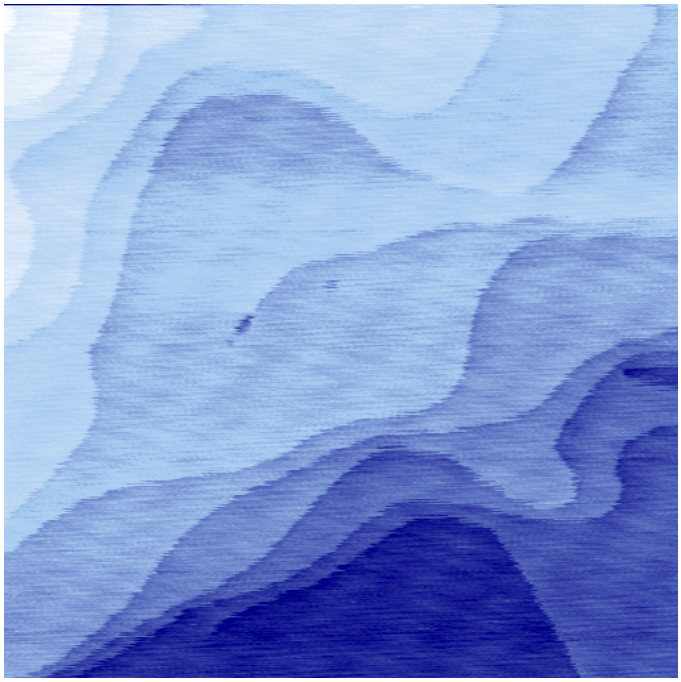

Figure 5.9: STM image of Au(111) recorded using a Au/polymer coaxial tip in a 12.1 keV beam chopped at 10 kHz in 800 mbar Ar, showing atomic steps. The topo/photo current separator was used to obtain the regular tunneling current, the input for the STM control system. Scanning parameters: 640 nm × 640 nm, ~1 nA (excluding offset current), -1 V, tip speed 2500 nm/s.

5.3.4 X-ray induced tunneling current enhancement

The most essential prerequisite in SXSTM measurements is the ability to measure the X-ray induced increase in the tunneling current, which provides the local X-ray absorption information [17,18]. To provide proof of this ability for our instrument, we measured the X-ray-induced current as a function of the regular tunneling current. Figure 5.10 shows the result as recorded on Au(111) in 800 mbar Ar. To obtain the topographic current, the slowly varying X-ray-induced offset current was subtracted from the tunneling current setpoint. The normalized photocurrent was obtained as (X-ray induced current - ion current background)/ion current background, where the ion current background was measured with the tip out of tunneling contact. As can be seen in Figure 5.10, the photocurrent correlates with the regular tunneling signal. This is expected, because the X-ray-induced modification of the tunneling current is assumed to arise from hot secondary electrons [18,38]. Most of the hot electrons do not have sufficient energy to escape from the sample into the vacuum, but they do have a much higher tunneling probability to the tip than electrons at the Fermi level. Still, this enhanced tunneling probability depends on the tip-sample distance, which changes when the topographic tunneling current setpoint is changed. Thus, the clear correlation between the photocurrent and the regular tunneling current provides a proof-of-principle of our ability to performed SXSTM measurements in a gas environment.

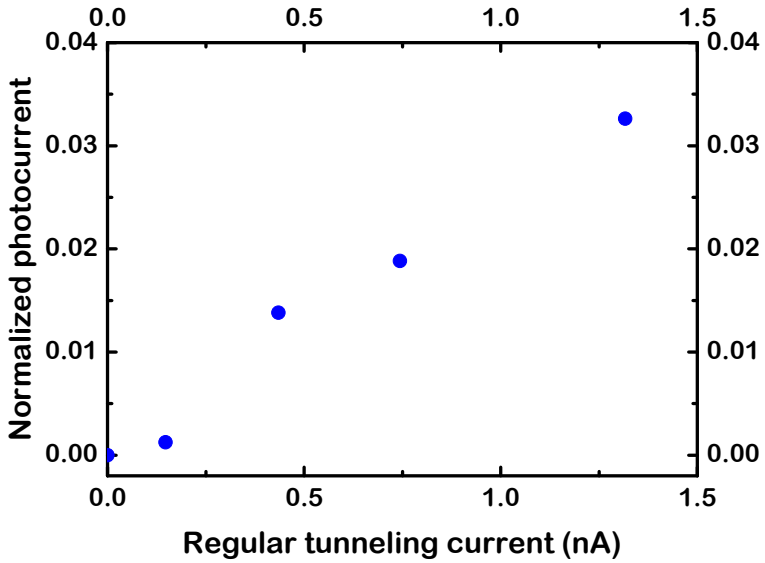

Figure 5.10: X-ray-induced current versus regular tunneling current, recorded on Au(111) in 800 mbar Ar using the topo/photo splitter with the 12.1 keV X-rays chopped at 10 kHz. The normalized photocurrent was obtained as (X-ray induced current-ion current background)/ion current background, where the ion current background was measured with the tip out of tunneling contact. Sample bias: -1 V, tip shield bias: 0 V.

5.4 Conclusion and outlook

We have developed an instrument suitable for performing local X-ray absorption measurements by modification of a previously developed high-pressure STM and X-ray scattering apparatus [14]. Several essential additions have been made in order to reach the required sensitivity to measure the small X-ray-induced modification of the tunneling current that carries the local X-ray absorption signal [17,18].

First, the STM is mounted on a new high-pressure cell with thin windows, providing high X-ray transparency in the energy range of interest, from 8 keV to 25 keV. Furthermore, we have shown that the beam shadow of the STM tip on a 2D X-ray detector can be used to align tip and beam with a precision of a few micrometer. Our measurements show that background currents from ions and photo-electrons cause much more severe signal distortions in a gas environment than in vacuum, particularly in the presence of insulating surfaces. We have therefore applied a Au coating to the high-pressure cell and employed coaxially shielded STM tips. The conductive outer layer of the coaxial tips can be biased to provide additional ion deflection. To separate the regular, 'topographic' tunneling current from the X-ray-induced current, a new high-speed electronics circuit was developed. Using these technical implementations, the X-ray induced modification of the tunneling current was measured on Au(111) in 800 mbar Ar. Combining our methodology with the knowledge of the spatial and chemical resolution of SXSTM developed in the literature [17,18], *operando* X-ray absorption measurements with nanometer spatial resolution have now come within reach.

References

[1] A.I. Frenkel, J.A. Rodriguez, J.G. Chen, Synchrotron techniques for in situ catalytic studies: Capabilities, challenges, and opportunities, ACS Catal. 2 (2012) 2269–2280.

[2] C.R.A. Catlow, Synchrotron radiation techniques in materials and environmental science, Philos. Trans. R. Soc. A. 373 (2015) 20130162.

[3] K. Devloo-Casier, K.F. Ludwig, C. Detavernier, J. Dendooven, In situ synchrotron based x-ray techniques as monitoring tools for atomic layer deposition, J. Vac. Sci. Technol. A Vacuum, Surfaces, Film. 32 (2014) 010801.

[4] S. Rackwitz, I. Faus, B. Lägel, J. Linden, J. Marx, E. Oesterschulze, K. Schlage, H.C. Wille, S. Wolff, J.A. Wolny, V. Schünemann, Installation of a combined Raman and AFM microscope as a sample environment for nuclear resonance scattering at P01, PETRA III, Hyperfine Interact. 226 (2014) 667–671.

[5] M. V Vitorino, A. Panzarella, L. Porcar, F. Carla, M. Boilot, S. Guerber, P. Bernard, M.S. Rodrigues, F. Sanz, M.I. Giannotti, L. Costa, Custom AFM for X-ray beamlines : in situ biological investigations under physiological conditions research papers, J. Synchrotron Radiat. 22 (2015) 1364–1371.

[6] T. Slobodskyy, a. V. Zozulya, R. Tholapi, L. Liefeith, M. Fester, M. Sprung, W. Hansen, Versatile atomic force microscopy setup combined with micro-focused X-ray beam, Rev. Sci. Instrum. 86 (2015) 065104.

[7] I. Schmid, J. Raabe, B. Sarafimov, C. Quitmann, S. Vranjkovic, Y. Pellmont, H.J. Hug, Coaxial arrangement of a scanning probe and an X-ray microscope as a novel tool for nanoscience, Ultramicroscopy. 110 (2010) 1267–1272.

[8] M.S. Rodrigues, O. Dhez, S. Le Denmat, J. Chevrier, R. Felici, F. Comin, S. Le Denmat, Local detection of X-ray spectroscopies with an in-situ Atomic Force Microscope, J. Instrum. 3 (2008) P12004–P12004.

[9] Z. Ren, F. Mastropietro, A. Davydok, S. Langlais, M.-I. Richard, J.-J. Furter, O. Thomas, M. Dupraz, M. Verdier, G. Beutier, P. Boesecke, T.W. Cornelius, Scanning force microscope for *in situ* nanofocused X-ray diffraction studies, J. Synchrotron Radiat. 21 (2014) 1128–1133.

[10] M.L. Cummings, T.Y. Chien, C. Preissner, V. Madhavan, D. Diesing, M. Bode, J.W. Freeland, V. Rose, Combining scanning tunneling microscopy and synchrotron radiation for high-resolution imaging and spectroscopy with chemical, electronic, and magnetic contrast, Ultramicroscopy. 112 (2012) 22–31.

[11] A. Saito, J. Maruyama, K. Manabe, K. Kitamoto, K. Takahashi, K. Takami, M. Yabashi, Y. Tanaka, D. Miwa, M. Ishii, Y. Takagi, M. Akai-Kasaya, S. Shin, T. Ishikawa, Y. Kuwahara, M. Aono, Development of a scanning tunneling microscope for in situ experiments with a synchrotron radiation hard-X-ray microbeam, J. Synchrotron Radiat. 13 (2006) 216–220.

[12] T. Matsushima, T. Okuda, T. Eguchi, M. Ono, A. Harasawa, T. Wakita, A. Kataoka, M. Hamada, A. Kamoshida, Y. Hasegawa, T. Kinoshita, Development and trial measurement of synchrotron-radiation-light- illuminated scanning tunneling microscope, Rev. Sci. Instrum. 75 (2004) 2149–2153.

[13] K. Tsuji, K. Wagatsuma, K. Sugiyama, K. Hiraga, Y. Waseda, EXAFS- and XANES-like Spectra Obtained by X-ray-excited Scanning Tunneling Microscope Tip

Current Measurement, Surf. Interface Anal. 27 (1999) 132–135.
[14] W.G. Onderwaater, P.C. van der Tuijn, R. V Mom, S.B. Roobol, M.A. van Spronsen, A. Saedi, J. Drnec, H. Isern, F. Carla, T. Dufrane, R. Koehler, B. Crama, I.M.N. Groot, R. Felici, J.W.M. Frenken, Combined scanning probe microscopy and X-ray scattering instrument for in situ catalysis investigations, Rev. Sci. Instrum. (2016) accepted.
[15] M.S. Rodrigues, T.W. Cornelius, T. Scheler, C. Mocuta, A. Malachias, R. Magalhães-Paniago, O. Dhez, F. Comin, T.H. Metzger, J. Chevrier, In situ observation of the elastic deformation of a single epitaxial SiGe crystal by combining atomic force microscopy and micro x-ray diffraction, J. Appl. Phys. 106 (2009) 103525.
[16] C. Leclere, T.W. Cornelius, Z. Ren, A. Davydok, J.S. Micha, O. Robach, G. Richter, L. Belliard, O. Thomas, In situ bending of an Au nanowire monitored by micro Laue diffraction, J. Appl. Crystallogr. 48 (2015) 291–296.
[17] N. Shirato, M. Cummings, H. Kersell, Y. Li, B. Stripe, D. Rosenmann, S.W. Hla, V. Rose, Elemental fingerprinting of materials with sensitivity at the atomic limit, Nano Lett. 14 (2014) 6499–6504.
[18] T. Okuda, T. Eguchi, K. Akiyama, A. Harasawa, T. Kinoshita, Y. Hasegawa, M. Kawamori, Y. Haruyama, S. Matsui, Nanoscale chemical imaging by scanning tunneling microscopy assisted by synchrotron radiation, Phys. Rev. Lett. 102 (2009) 105503.
[19] T. Eguchi, T. Okuda, T. Matsushima, A. Kataoka, A. Harasawa, K. Akiyama, T. Kinoshita, Y. Hasegawa, M. Kawamori, Y. Haruyama, S. Matsui, Element specific imaging by scanning tunneling microscopy combined with synchrotron radiation light, Appl. Phys. Lett. 89 (2006) 243119.
[20] A. Saito, K. Takahashi, Y. Takagi, K. Nakamatsu, K. Hanai, Y. Tanaka, D. Miwa, M. Akai-kasaya, S. Shin, S. Matsui, T. Ishikawa, Y. Kuwahara, M. Aono, Study for noise reduction in synchrotron radiation based scanning tunneling microscopy by developing insulator-coat tip, Surf. Sci. 601 (2007) 5294–5299.
[21] K. Akiyama, T. Eguchi, T. An, Y. Hasegawa, T. Okuda, A. Harasawa, T. Kinoshita, Fabrication of a glass-coated metal tip for synchrotron-radiation-light-irradiated scanning tunneling microscopy, Rev. Sci. Instrum. 76 (2005) 1–3.
[22] H. Yan, M. Cummings, F. Camino, W. Xu, M. Lu, X. Tong, N. Shirato, D. Rosenmann, V. Rose, E. Nazaretski, Fabrication and characterization of CNT-based smart tips for synchrotron assisted STM, J. Nanomater. 2015 (2015) 492657.
[23] V. Rose, T.Y. Chien, J. Hiller, D. Rosenmann, R.P. Winarski, X-ray nanotomography of SiO2-coated Pt90Ir 10 tips with sub-micron conducting apex, Appl. Phys. Lett. 99 (2011) 173102.
[24] K. Wang, D. Rosenmann, M. Holt, R. Winarski, S.W. Hla, V. Rose, An easy-to-implement filter for separating photo-excited signals from topography in scanning tunneling microscopy, Rev. Sci. Instrum. 84 (2013) 063704.
[25] R. Van Rijn, M.D. Ackermann, O. Balmes, T. Dufrane, A. Geluk, H. Gonzalez, H. Isern, E. De Kuyper, L. Petit, V.A. Sole, D. Wermeille, R. Felici, J.W.M. Frenken, Ultrahigh vacuum/high-pressure flow reactor for surface x-ray diffraction and

grazing incidence small angle x-ray scattering studies close to conditions for industrial catalysis, Rev. Sci. Instrum. 81 (2010) 014101.
[26] M.J. Rost, L. Crama, P. Schakel, E. Van Tol, G.B.E.M. Van Velzen-Williams, C.F. Overgauw, H. Ter Horst, H. Dekker, B. Okhuijsen, M. Seynen, A. Vijftigschild, P. Han, A.J. Katan, K. Schoots, R. Schumm, W. Van Loo, T.H. Oosterkamp, J.W.M. Frenken, Scanning probe microscopes go video rate and beyond, Rev. Sci. Instrum. 76 (2005) 053710.
[27] C.T. Herbschleb, P.C. van der Tuijn, S.B. Roobol, V. Navarro, J.W. Bakker, Q. Liu, D. Stoltz, M.E. Cañas-Ventura, G. Verdoes, M.A. van Spronsen, M. Bergman, L. Crama, I. Taminiau, A. Ofitserov, G.J.C. van Baarle, J.W.M. Frenken, The ReactorSTM: atomically resolved scanning tunneling microscopy under high-pressure, high-temperature catalytic reaction conditions., Rev. Sci. Instrum. 85 (2014) 083703.
[28] S.B. Roobol, M.E. Cañas-Ventura, M. Bergman, M.A. Van Spronsen, W.G. Onderwaater, P.C. Van Der Tuijn, R. Koehler, A. Ofitserov, G.J.C. Van Baarle, J.W.M. Frenken, The ReactorAFM: Non-contact atomic force microscope operating under high-pressure and high-temperature catalytic conditions, Rev. Sci. Instrum. 86 (2015) 033706.
[29] J.C.D. B.L. Henke, E.M. Gullikson, X-Ray Interactions: Photoabsorption, Scattering, Transmission, and Reflection at E = 50-30,000 eV, Z = 1-92, At. Data Nucl. Data Tables. 54 (1993) 181–324.
[30] S.J. Schowalter, C.B. Connolly, J.M. Doyle, Permeability of noble gases through Kapton, butyl, nylon, and "Silver Shield," Nucl. Instruments Methods Phys. Res. Sect. A Accel. Spectrometers, Detect. Assoc. Equip. 615 (2010) 267–271.
[31] S.L.M. Schroeder, G.D. Moggridge, R.M. Ormerod, T. Rayment, R.M. Lambert, What determines the probing depth of electron yield XAS?, Surf. Sci. 324 (1995) L371–L377.
[32] S.L.M. Schroeder, G.D. Moggridge, T. Rayment, R.M. Lambert, In situ probing of the near-surface properties of heterogeneous catalysts under reaction conditions: An introduction to total electron-yield XAS, J. Mol. Catal. A Chem. 119 (1997) 357–365.
[33] W.J. Miloch, S. V. Vladimirov, Charging of spinning insulating objects by plasma and photoemission, Geophys. Res. Lett. 36 (2009) L18110.
[34] M. Salmeron, R. Schlögl, Ambient pressure photoelectron spectroscopy: A new tool for surface science and nanotechnology, Surf. Sci. Rep. 63 (2008) 169–199.
[35] D.E. Starr, Z. Liu, M. Hävecker, A. Knop-Gericke, H. Bluhm, Investigation of solid/vapor interfaces using ambient pressure X-ray photoelectron spectroscopy., Chem. Soc. Rev. 42 (2013) 5833–57.
[36] A.J. Bard, M. V. Mirkin, Scanning Electrochemical Microscopy, CRC Press, 6000 Broken Sound Parkway, Boca Raton, United States, 2012.
[37] C. Ponchut, J.M. Rigal, J. Clément, E. Papillon, A. Homs, S. Petitdemange, MAXIPIX, a fast readout photon-counting X-ray area detector for synchrotron applications, J. Instrum. 6 (2011) C01069–C01069.
[38] C.Y. Chiu, Y.L. Chan, Y.J. Hsu, D.H. Wei, Collecting photoelectrons with a scanning tunneling microscope nanotip, Appl. Phys. Lett. 92 (2008) 103101.